Chapter 17

Modern Technologies for Creating Nanostructures in Thin-Film Solar Cells

Yang Tang

Additional information is available at the end of the chapter

http://dx.doi.org/10.5772/64611

Abstract

Most photovoltaic devices (solar cells) sold in the market today are based on silicon wafers, so-called first-generation technology. There is an argument whether the market at present is on the verge of switching to a "second generation" of thin-film solar cell technology. Thin-film photovoltaic device technology relies on light management to enhance light absorption in thin absorber layers. The use of the ZnO nanorods in the thin-film solar cells is an effective way to decrease the reflection. The variation of the geometrical parameters of the ZnO nanorods, such as the diameter, the height and the density, can lead to an optimum, which results in the maximal absorption in the absorber.

Keywords: thin film, solar cell, nanostructure, electrodeposition, efficiency

1. Introduction

The solar energy as one of the new energy sources and a regenerated energy is abundant and pollution free. Most photovoltaic devices (solar cells) sold in the market today are based on silicon wafers, so-called first-generation technology. There is an argument that whether the market at present is on the verge of switching to a "second generation" of thin-film solar cell technology. Nowadays three types of the thin-film solar cells have realized industrialization. They are copper indium gallium selenide (CIGS) solar cells, CdTe solar cells and a-Si solar cells. CIGS-based thin-film photovoltaic devices show the highest efficiency among the various thin-film technologies, having recently reached a record value of 22.6% for the laboratory scale [1]. CdTe-based thin-film solar cells have got a record lab efficiency of 22.1% [2]. Some of the technologies have already entered the stage of mass production with commercial modules that provide stable efficiencies in the 13–14% range. There is still a large gap between the lab-scale

efficiency and the module efficiency indicating the great potential of the technologies. It is vitally important to further develop the innovative thin-film technologies using environmentally friendly and sustainable approaches with lower costs and higher efficiencies.

2. Nanostructured thin-film solar cells

This section starts with a brief introduction on ZnO fundamental properties and the definition of nanostructures. The structures of the thin-film photovoltaic devices are depicted. Then the nanorod meets the solar cell. The applications of the ZnO nanorods in thin-film photovoltaic devices are given. It is followed by the results on the efficiency boost of the thin-film solar cells implanted with ZnO nanorods.

2.1. Implantation of the nanostructures

ZnO is a wide direct bandgap II–VI semiconductor. In last decade, the ZnO material ranging from its thin films to nanostructures has been widely investigated for their applications in various electronic and optoelectronic devices. ZnO is not really a newly discovered material. Research on ZnO has continued for many decades with interest. In terms of its characterization, reports go back to 1935 or even earlier. For example, lattice parameters of ZnO were investigated for many decades [3–7].

Most of the group II–VI binary compound semiconductors crystallize in either cubic zinc blende or hexagonal wurtzite structure where each anion is surrounded by four cations at the corners of a tetrahedron and vice versa. Three kinds of crystal structures are shared by ZnO, which are rocksalt, zinc blende and wurtzite [8]. The zinc blende ZnO structure can be stabilized only by growth on cubic substrates, and the rocksalt structure may be obtained at relatively high pressures [8].

In a variant of the cell structure the nontransparent rear metal contact can be replaced by a transparent conductive oxides (TCO) film. For conventional CIGS thin-film solar cells, metallic Mo back electrodes are commonly used, making it impossible for light to pass through the metal electrode layer. It is possible to reverse the cell structure by starting with the deposition of the transparent contact (superstrate configuration). ZnO nanorod arrays are embedded between the TCO layer and the absorber layer serving as a buffer role. Optionally, an additional buffer layer can be inserted between the ZnO nanorods and the absorber in the superstrate solar cells. The light enters the cell through the superstrate, which has the advantage that the module can be encapsulated with nontransparent material of lower mass and lower cost. Moreover, if the other contact electrode were replaced by a TCO contact, the cell would be illuminated by both sides. In addition, the ZnO nanorod arrays have been incorporated into a superstrate or a bifacial cell structure of the other thin-film photovoltaic devices such as dye-sensitized solar cells [9], quantum dye-sensitized solar cells [10] and organic solar cells [11].

2.2. Efficiency boost of the nanostructured thin-film solar cells

The ZnO nanorods electrodeposited on fluorine doped tin oxide (FTO) substrates have a typical bottom diameter of 220 nm and a top diameter of 120 nm. The ZnO nanorod arrays' density is 6.8×10^8 1/cm^2. The simulation of the nanostructured structure started with the

ZnO nanorod arrays possessing this typical morphology and geometry. The modeling results including reflectance, transmission and absorption were weighted with the AM 1.5 solar spectrum. The optical modeling results on the structure of glass/SnO_2:F/ZnO nanorods/Cu(In,Ga)Se_2. The optical constants of the Cu(In,Ga)Se_2 is derived from the layer. At first, The ZnO nanorod arrays' densities were varied while the other parameters such as the diameters and lengths are fixed. **Table 1** and **Figure 1** show the modeling results. The densities are varied from 4.2×10^8 to 3.2×10^9 1/cm^2. Correspondingly, the percentage site coverages of the ZnO nanorods on the FTO surface are varied from 13.2 to 100%. As shown in the table, an increase in the ZnO nanorods' density leads to a considerable decrease in the reflection. The reflection is decreased from 12.07 to 5.60% by increasing the ZnO nanorods' density from 4.2×10^8 1/cm^2 (site coverage 13.2%) to 3.2×10^9 1/cm^2 (site coverage 100%). An increase in the ZnO nanorods' density results in an increase in the transmission. With increasing the ZnO nanorods' density from 4.2×10^8 1/cm^2 (site coverage 13.2%) to 3.2×10^9 1/cm^2 (site coverage 100%), the transmission is increased from 3.33 to 4.36%. The reason for the increase of the transmission in the range between 900 and 1200 nm is that ZnO nanorods work as a waveguide for the infrared light. As a result of the rise in the ZnO nanorods' density from 4.2×10^8 1/cm^2 (site coverage 13.2%) to 3.1×10^9 1/cm^2 (site coverage 97.5%), the absorption in SnO_2:F descends from 12.15 to 11.09%. However, the absorption in the SnO_2:F ascends from 11.09 to 11.58% with increasing the ZnO nanorods' density from 3.1×10^9 1/cm^2 (site coverage 97.5%) to 3.2×10^9 1/cm^2 (site coverage 100.0%). An increase in the ZnO nanorods' density leads to a continuous increase of the absorption in ZnO nanorods. Owing to the decrease of the reflection and the SnO_2:F absorption with increasing the ZnO nanorods' density from 4.2×10^8 1/cm^2 (site coverage 13.2%) to 3.1×10^9 1/cm^2 (site coverage 97.5%), the absorption in Cu(In,Ga)Se_2 is boosted from 63.30 to 68.13%. An increase in the ZnO nanorods' density over 3.1×10^9 1/cm^2 results in a reduction in the absorption of Cu(In,Ga)Se_2. Therefore, the structure with the ZnO nanorods' density of 3.1×10^9 1/cm^2 (site coverage 97.5%) has the maximum absorption in Cu(In,Ga)Se_2.

Sample	ZnO nanorods' height (mm)	Reflection (%)	Transmission (%)	Absorption in Sn_2O_3:F (%)	Absorption in ZnO nanorods (%)	Absorption in Cu(In,Ga)Se_2 (%)
1	–	13.18	3.47	12.27	–	62.20
2	50	8.30	3.54	11.75	1.01	66.52
3	90	5.97	3.77	11.34	1.45	68.59
4	100	5.88	3.83	11.28	1.48	68.65
5	110	5.86	3.90	11.24	1.50	68.62
6	200	5.93	4.08	11.18	1.73	68.20
7	300	5.70	4.31	11.09	1.89	68.13
8	400	5.72	4.64	10.98	2.02	67.76
9	700	5.65	5.39	10.88	2.31	66.89
10	1000	5.74	6.02	10.95	2.58	65.83

Table 1. The optical modeling results on the structure of glass/SnO_2:F/ZnO nanorods/Cu(In,Ga)Se_2. The simulated ZnO nanorod has a bottom diameter of 220 nm and a top diameter of 120 nm. The density of the nanorods is 3.1×10^9 1/cm^2 with the site coverage of 97.5%. The heights of the ZnO nanorods are varied.

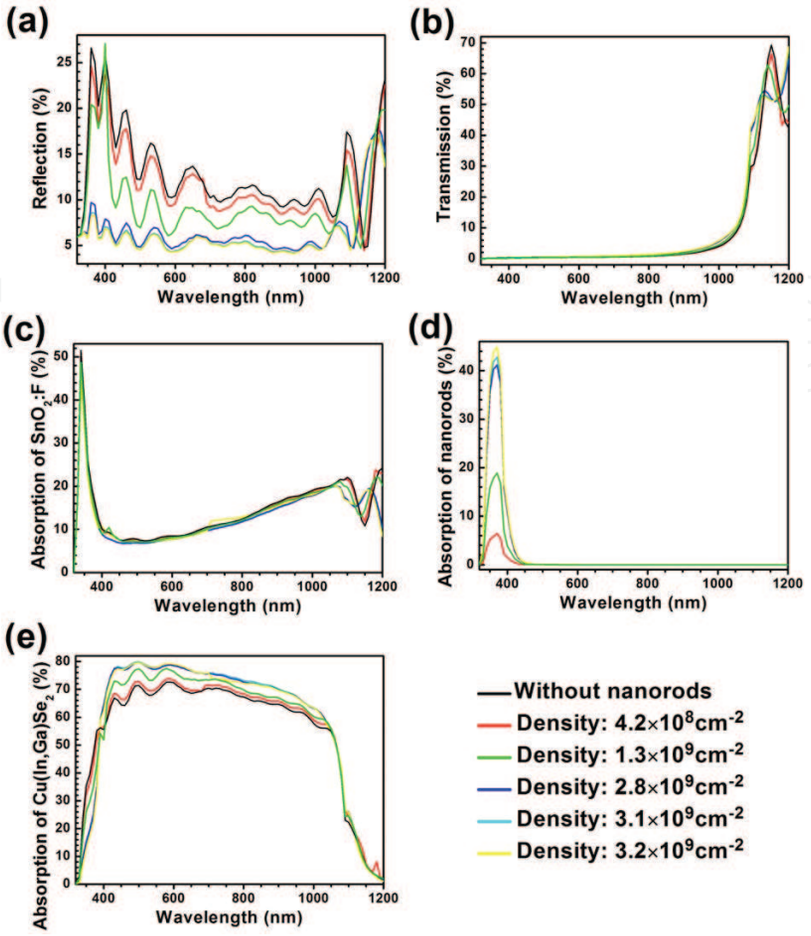

Figure 1. The simulated optical spectra of the structure of glass/SnO_2:F/ZnO nanorods/Cu(In,Ga)Se_2. The simulated ZnO nanorod has a bottom diameter of 220 nm and a top diameter of 120 nm. The nanorod's height is 300 nm. The densities of the ZnO nanorod arrays are varied. Correspondingly the percentage site coverages of the ZnO nanorods on the SnO_2:F surface are varied.

Since the ZnO nanorods' density has been optimized to be 3.1 × 10^9 1/cm^2 (site coverage 97.5%), the other morphological parameters of the ZnO nanorods would be varied to achieve the maximum absorption in Cu(In,Ga)Se_2. Thus, the ZnO nanorods' heights are varied while the other parameters such as the diameters and densities are fixed. **Table 2** and **Figure 2** show the modeling results. The nanorods' heights are varied from 50 to 1000 nm. By increasing the ZnO nanorods' height from 50 to 110 nm, the reflection of the structure is decreased from 8.30 to 5.86%, which is diminished by 29.4%. An increase in the ZnO nanorods' heights from 110 to 1000 nm does not induce a significant change of the structures' reflections and the reflections vary in a small range between 5.65 and 5.93%. As shown in **Table 2**, an increase in the ZnO nanorods' height leads to a considerable increase of the structure's transmission. The transmission is boosted from 3.57 to 6.02% by increasing the ZnO nanorods' height from 50 to 1000 nm, which is enlarged by 68.6%. As shown in **Figure 2**, the increase in the transmission is in the range from 900 (1.38 eV) to 1200 nm (1.03 eV), because ZnO nanorods work as a waveguide enhancing the infrared transmission. An increase in the ZnO nanorods' height from 50 to 700 nm induces a slight decrease of the absorption in SnO_2:F from 11.75 and 10.88%, which is diminished by 7.4%. However, the absorption in the SnO_2:F ascends from 10.88 to 10.95% with increasing the ZnO nanorods' height from 700 to 1000 nm. An

increase in the ZnO nanorods' height leads to a continuous increase of the absorption in ZnO nanorods. The absorption in ZnO nanorods ascends from 1.01 to 2.58% as a result of the increase in the nanorods' height from 50 to 1000 nm. Owing to the decrease of the reflection and the SnO_2:F absorption with increasing the ZnO nanorods' height from 50 to 100 nm, the absorption in Cu(In,Ga)Se_2 is boosted from 66.52 to 68.65%. As a consequence of the boost in the transmission and the ZnO nanorod absorption, an increase in the ZnO nanorods' height over 100 nm results in a reduction in the absorption of Cu(In,Ga)Se_2. Therefore, the nanostructured thin-film solar cells with the ZnO nanorods' height of 100 nm has the maximum absorption in Cu(In,Ga)Se_2.

Sample	ZnO nanorods' bottom diameter (nm)	Nanorod site coverage (%)	Reflection (%)	Transmission (%)	Absorption in Sn_2O_3:F (%)	Absorption in ZnO nanorods (%)	Absorption in Cu(In,Ga)Se_2 (%)
1	–	–	13.18	3.47	12.27	–	62.20
2	120	29.9	10.31	3.66	11.81	0.43	64.91
3	160	53.2	8.39	3.73	11.56	0.89	66.55
4	200	89.7	6.55	3.81	11.35	1.31	68.10
5	210	94.2	6.18	3.82	11.31	1.38	68.43
6	220	97.5	5.88	3.83	11.28	1.48	68.65

Table 2. The optical modeling results on the structure of glass/SnO_2:F/ZnO nanorods/Cu(In,Ga)Se_2. The simulated ZnO nanorod has a top diameter of 120 nm and a length of 100 nm. The density of the ZnO nanorod arrays is 3.1×10^9 1/cm^2. The bottom diameters of the ZnO nanorod are varied. Correspondingly the percentage site coverages of the ZnO nanorods on the SnO_2:F surface are varied.

First, the ZnO nanorods' bottom diameters are varied while the other parameters such as the top diameter, length and density are fixed. **Table 3** and **Figure 3** show the modeling results. The nanorods' bottom diameters are varied from 120 to 220 nm. Correspondingly, the percentage site coverage of the ZnO nanorods on the FTO surface is varied from 29.9 to 97.5%. As shown in the table, the ZnO nanorod possessing the same size of the bottom and top diameters has the hexagonal prism morphology and shows a high reflection of 10.31%. An increase in the ZnO nanorods' bottom diameter leads to a considerable decrease in the reflection. By increasing the ZnO nanorods' bottom diameter from 120 (site coverage 29.9%) to 220 nm (site coverage 97.5%), the reflection is decreased from 10.31 to 5.88%, which is reduced by 43.0%. With increasing the ZnO nanorods' bottom diameter from 120 (site coverage 29.9%) to 220 nm (site coverage 97.5%), the transmission is slightly increased from 3.66 to 3.83%. As a result of the rise in the ZnO nanorods' bottom diameter from 120 (site coverage 29.9%) to 220 nm (site coverage 97.5%), the absorption in SnO_2:F descends from 11.81 to 11.28%. An increase in the ZnO nanorods' bottom diameter leads to a continuous increase of the absorption in ZnO nanorods. Owing to the decrease of the reflection and the SnO_2:F absorption with increasing the ZnO nanorods' bottom diameter from 120 (site coverage 29.9%) to 220 nm (site coverage 97.5%), the absorption in Cu(In,Ga)Se2 is boosted from 64.91 to 68.65%. Therefore, the nanostructured thin-film solar cells with the ZnO nanorods' bottom diameter of 220 nm (site coverage 97.5%) has the maximum absorption in Cu(In,Ga)Se_2.

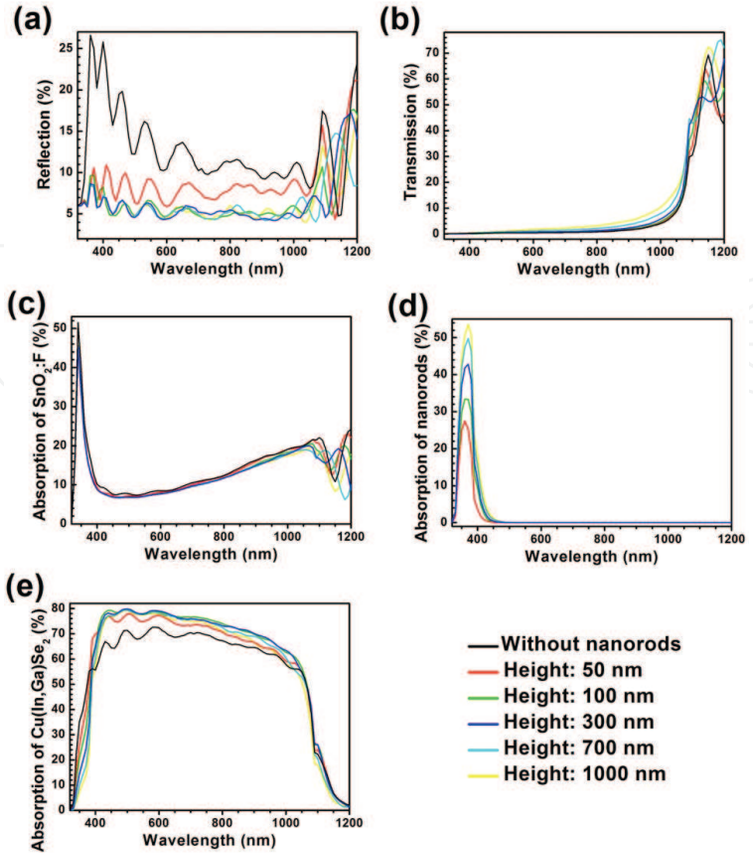

Figure 2. The simulated optical spectra of the structure of glass/SnO_2:F/ZnO nanorods/Cu(In,Ga)Se_2. The simulated ZnO nanorod has a bottom diameter of 220 nm and a top diameter of 120 nm. The density of the nanorods is 3.1 × 10^9 1/cm^2 with the site coverage of 97.5%. The heights of the ZnO nanorod are varied.

Since the ZnO nanorods' bottom diameter has been optimized to be 220 nm, the top diameter of the ZnO nanorods would be varied to achieve the maximum absorption in Cu(In,Ga)Se_2. **Table 4** and **Figure 4** show the modeling results. The nanorods' top diameters are varied from 80 to 160 nm. With increasing the ZnO nanorods' top diameter from 80 to 150 nm, the reflection of the structure is decreased from 6.85 to 5.64%, which is diminished by 17.7%. As shown in **Table 4** an increase in the ZnO nanorods' top diameter over 150 nm results in a slight increase in the reflection. The reflection of the structure with the ZnO nanorods possessing a top diameter of 160 nm is 5.65%. By increasing the ZnO nanorods' top diameter from 80 to 160 nm, the transmission is increased from 3.67 to 3.96%. As a result of the rise in the ZnO nanorods' top diameter from 80 to 160 nm, the absorption in SnO_2:F descends from 11.48 to 11.18%. An increase in the ZnO nanorods' top diameter leads to a continuous increase of the absorption in ZnO nanorods. Owing to the decrease of the reflection and the SnO_2:F absorption with increasing the ZnO nanorods' top diameter from 80 to 140 nm, the absorption in Cu(In,Ga)Se_2 is boosted from 67.84 to 68.76%. By increasing the ZnO nanorods' top diameter from 140 to 150 nm, the absorption in Cu(In,Ga)Se_2 keeps constant. An increase in the ZnO nanorods' top diameter over 150 nm results in a reduction in the absorption of Cu(In,Ga)Se_2. Therefore, the nanostructured thin-film solar cells with the ZnO nanorods' top diameter of 150 nm has the maximum absorption in Cu(In,Ga)Se_2. Compared with the structure without using the ZnO nanorods, the absorption of Cu(In,Ga)Se_2 in the nanorod-integrated structure is boosted from 62.20 to 68.76%, which is enlarged by 9.5%.

http://dx.doi.org/10.5772/64611

Sample	ZnO nanorods' top diameter (nm)	Reflection (%)	Transmission (%)	Absorption in Sn_2O_3:F (%)	Absorption in ZnO nanorods (%)	Absorption in Cu(In,Ga)Se_2 (%)
1	–	13.18	3.47	12.27	–	62.20
2	60	6.85	3.67	11.48	1.28	67.84
3	80	6.48	3.73	11.41	1.34	68.16
4	100	6.15	3.78	11.35	1.40	68.44
5	120	5.88	3.83	11.28	1.48	68.65
6	130	5.77	3.87	11.25	1.51	68.72
7	140	5.69	3.90	11.22	1.55	68.76
8	150	5.64	3.93	11.20	1.59	68.76
9	160	5.65	3.96	11.18	1.62	68.71

Table 3. The optical modeling results on the structure of glass/SnO_2:F/ZnO nanorods/Cu(In,Ga)Se_2. The simulated ZnO nanorod has a bottom diameter of 220 nm and a height of 100 nm. The density of the ZnO nanorod arrays is 3.1×10^9 1/cm^2. The top diameters of the ZnO nanorods are varied.

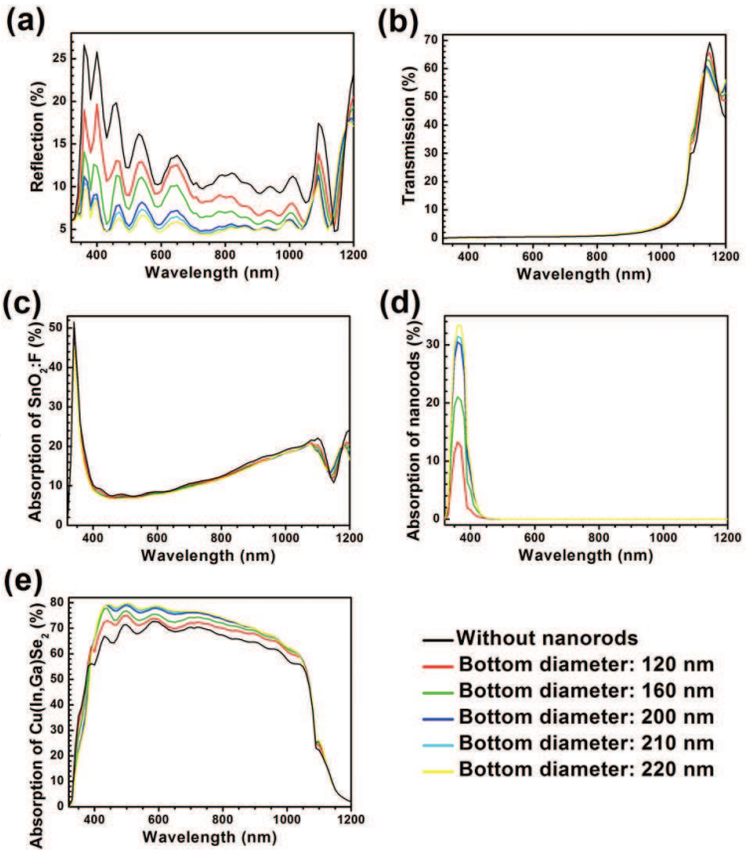

Figure 3. The simulated optical spectra of the structure of glass/SnO_2:F/ZnO nanorods/Cu(In,Ga)Se_2. The simulated ZnO nanorod has a top diameter of 120 nm and a height of 100 nm. The density of the ZnO nanorod arrays is 3.1×10^9 1/cm^2. The bottom diameters of the ZnO nanorod are varied. Correspondingly the percentage site coverages of the ZnO nanorods on the SnO_2:F surface are varied.

Sample	ZnO nanorods' top diameter (nm)	Reflection (%)	Transmission (%)	Absorption in Sn_2O_3:F (%)	Absorption in ZnO nanorods (%)	Absorption in Cu(In,Ga)Se_2 (%)
1	–	13.18	3.47	12.27	–	62.20
2	60	6.85	3.67	11.48	1.28	67.84
3	80	6.48	3.73	11.41	1.34	68.16
4	100	6.15	3.78	11.35	1.40	68.44
5	120	5.88	3.83	11.28	1.48	68.65
6	130	5.77	3.87	11.25	1.51	68.72
7	140	5.69	3.90	11.22	1.55	68.76
8	150	5.64	3.93	11.20	1.59	68.76
9	160	5.65	3.96	11.18	1.62	68.71

Table 4. The optical modeling results on the structure of glass/SnO_2:F/ZnO nanorods/Cu(In,Ga)Se_2. The simulated ZnO nanorod has a bottom diameter of 220 nm and a height of 100 nm. The density of the ZnO nanorod arrays is 3.1×10^9 1/cm^2. The top diameters of the ZnO nanorods are varied.

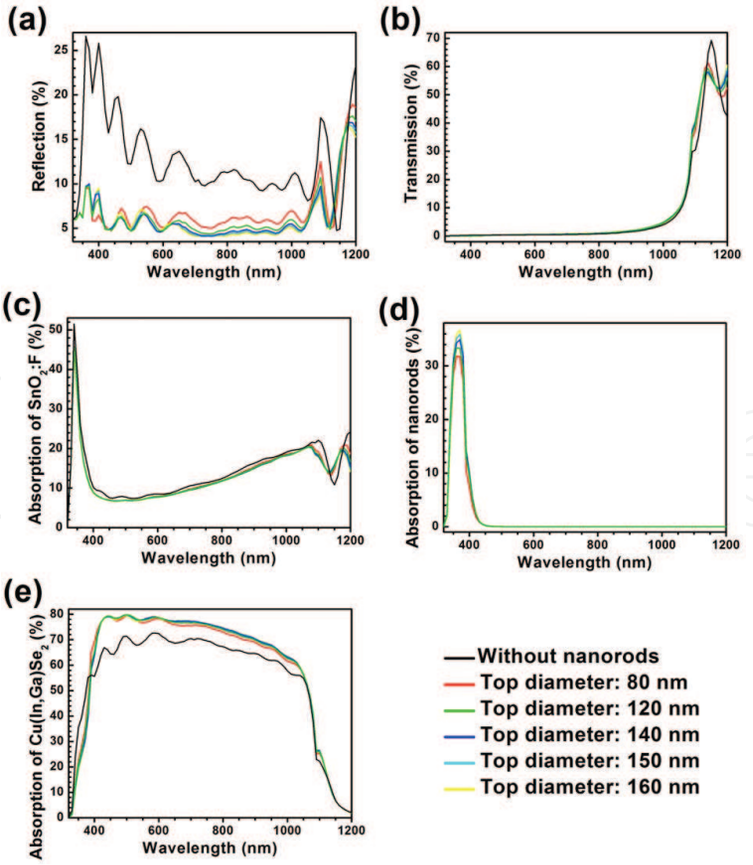

Figure 4. Current versus time transients obtained on FTO substrate at potential of −1.39 V.

http://dx.doi.org/10.5772/64611

3. Growth of ZnO nanorod arrays

The solution-based fabrication routes including hydrothermal method and electrochemical deposition (ECD) method are the ways to grow ZnO nanostructures at a low temperature down to the range between 60 and 90°C [12–23]. Meanwhile the growth can be achieved over large areas up to 30 × 30 cm. A two-stage electrodeposition method for tailoring the ZnO nanostructures is presented.

3.1. Nucleation and crystal growth

For the electrolyte recipe of ZnO nanostructures, there are two choices for the Zn source in the solution: $ZnCl_2$ [12] or $Zn(NO_3)_2$ [13]. In order to provide the oxygen source, one would have to bubble O_2 into the electrolyte during electrodeposition if $ZnCl_2$ were used [12]. The oxygen source is from the reduction of NO_3^- for the electrolyte using $Zn(NO_3)_2$. The formations of ZnO by NO_3^- precursors were described in Eqs. (1)–(4) as follows [13].

$$Zn\left(NO_3\right)_2 \rightarrow Zn^{2+} + 2NO_3^- \quad (1)$$

$$NO_3^- + 2e + H_2O \rightarrow 2OH^- + NO_2^- \quad (2)$$

$$Zn^{2+} + 2OH^- \rightarrow Zn(OH)_2 \quad (3)$$

$$Zn(OH)_2 \rightarrow ZnO + H_2O \quad (4)$$

During the ECD process, the electrodeposited products are deposited on one of the electrodes. The electrode with the deposited materials is the working electrode (WE). However, the WE is not adequate for the complete ECD process. At least another electrode should be installed for allowing current to flow. In the simplest case, a two-electrode cell is used for ECD. In order to measure the accurate WE potential, a three-electrode cell containing a WE, a counter electrode (CE) and a reference electrode (RE) is more common. A current flows between the WE and CE, while the potential of the WE is measured against the RE. The glass substrates are used as the WE. The electrochemical cell was placed in a thermoregulated bath. The liquid electrolyte contains the salts regarding the recipes. A schematic illustration of the set up for the ECD process is shown in **Figure 5**. The electrochemical process is controlled and recorded by a potentiostat/galvanostat.

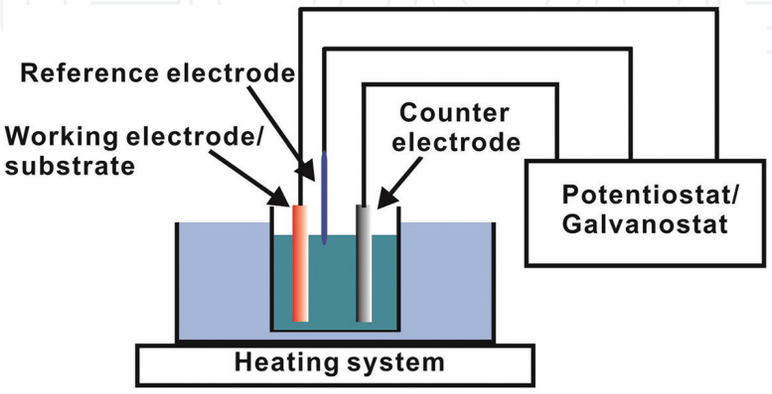

Figure 5. The scheme of the electrochemical deposition system.

Figure 6 shows a typical curve for current vs transit time obtained in the electrodeposition process of the ZnO nanorods. At the beginning of the potential step, there is a rapid surge of the current. The potential difference between the FTO surface and the electrolyte leads to the accumulation of excess charges near the surface. As a result, the electric double layer is formed at the phase boundary [24]. The initial surge corresponds to the electric double layer charging at the onset of the potential step [25]. After the surge, current decays abruptly as cations are reduced and the anions are oxidized in the close vicinity of the electrode [26, 27]. The nucleation forms in this stage. As fresh cations and anions diffuse, the current began to increase. The internal hexagonal structure of ZnO favors the anisotropic growth along the c-axis direction, which leads to the formation of the nanorods [28, 29]. During the nanorods' growth process, the surface area of the nanorods is increasing continuously. Therefore, the transient current density cannot be determined except for monitoring the in situ growth of the nanorods and collecting the information of the nanorods' morphological changes during the electrodeposition process.

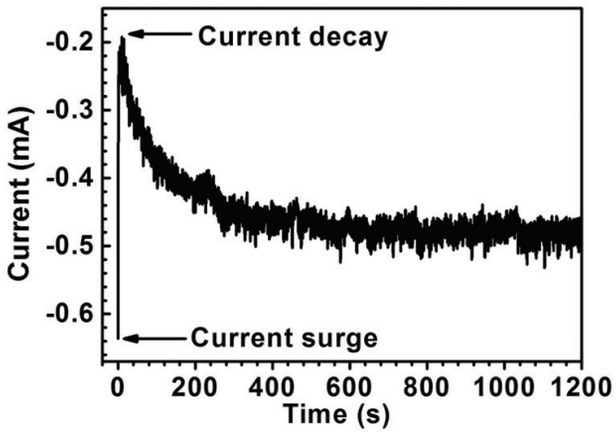

Figure 6. Current versus time transients obtained on FTO substrate at potential of −1.39 V.

3.2. Two-stage electrodeposition

Since the growth of ZnO nanostructures greatly depends on the nucleation process, it is possible to control the ZnO nanostructures' growth and properties by adjusting the amperage in the nucleation process. We developed a two-stage electrodeposition method to control the electrodeposited ZnO nanostructures' morphology and geometry. The samples were prepared from an aqueous solution: 7 mM $Zn(NO_3)_2.6H_2O$ and 7mM NH_4NO_3. The method was divided into two stages. A galvanic current (galvanic control) was applied during the first stage and then it was switched to a potentiostatic mode (−1.39V) (potentiostatic control) for the following growth stage. In order to investigate the influence of the galvanic current on the ZnO nanorods' growth and properties, we prepared one sample by using potentiostatic method (−1.39V) and the other samples by using two-stage electrodeposition method with the galvanic current ranging from −0.2 to −2 mA. All the FTO substrates were cut into small 2.5 cm^2 rectangles and then cleaned in an ultrasonic bath of acetone and ethanol with subsequent rinsing in distilled water. After preparation, the samples were washed with distilled water to remove any residual salt. By using this new method, the packing density of ZnO nanorods on bare FTO can be adjusted.

3.3. Control of ZnO nanorod arrays' density

Since the growth of ZnO nanorods greatly depends on the nucleation process, it is possible to control the ZnO nanostructures' growth and properties by adjusting the current density in the nucleation process. We developed a new method, that is, two-stage electrodeposition method to control the packing density and diameter of the electrodeposited ZnO nanorods. The two-stage eletrodeposition method was divided into two stages. A galvanic current was applied during the first stage and then it was switched to a potentiostatic mode for the following growth stage. In order to investigate the influence of the galvanic current density on the ZnO nanorods' growth and properties, we prepared one sample by using potentiostatic method with a potential of −1.39V and the other samples by using galvanic current ranging from −0.2 to −2 mA/cm^2.

The average density, average diameter the average length in five ZnO nanorods samples were estimated from a statistical evaluation and are summarized in **Table 5**. The diameter and height dispersion in five ZnO nanorod samples are shown in **Figure 7**. It shows that the ZnO nanorods' density in samples prepared by using two-stage eletrodeposition method with a high galvanic current density (−0.5 to −2 mA/cm^2) is larger than that of sample prepared under a low galvanic current density (−0.2 mA/cm^2). Therefore, it is clear that an increase in galvanic current density leads to a considerable increase of the ZnO nanorods' density. By increasing the galvanic current density from −0.2 to −2 mA/cm^2, the density of ZnO nanorods was boosted from 4.2 × 10^8 to 1.3 × 10^9 1/cm^2, which is enlarged by ~200%. According to the formations of ZnO by NO_3^- precursors described in Eqs. (1)–(4), an increase in a current raises the yields of OH^- ions. As a result, the nucleation sites were boosted in the initial nucleation process. The mechanism is illustrated in **Figure 8**. The ZnO nanorods' density was increased in the following process under the potentiostatic mode.

Galvanostatic stage: current density (mA/cm^2)	Potentiostatic stage: potential (V)	Average diameter (nm)	Average height (nm)	Density (10^8/cm^2)
0	−1.39	166	619	6.8
−0.2	−1.39	317	625	4.2
−0.5	−1.39	82	625	9.1
−1.2	−1.39	82	622	13.0
−2	−1.39	74	620	12.9

Table 5. Growth parameters of two stages, average diameter, average height and density of the ZnO nanorods.

In order to investigate the nucleation process at the galvanic stage, four samples were prepared under a galvanic mode with the galvanic current density ranging from −0.2 to −2 mA/cm^2, and the process was stopped before the following potentiostatic stage. The densities of the nucleation sites in these samples were shown in **Table 6**. The size of nuclei sites in the sample prepared under −0.2 mA/cm^2 was too small to be observed in the measurements. By increasing the galvanic

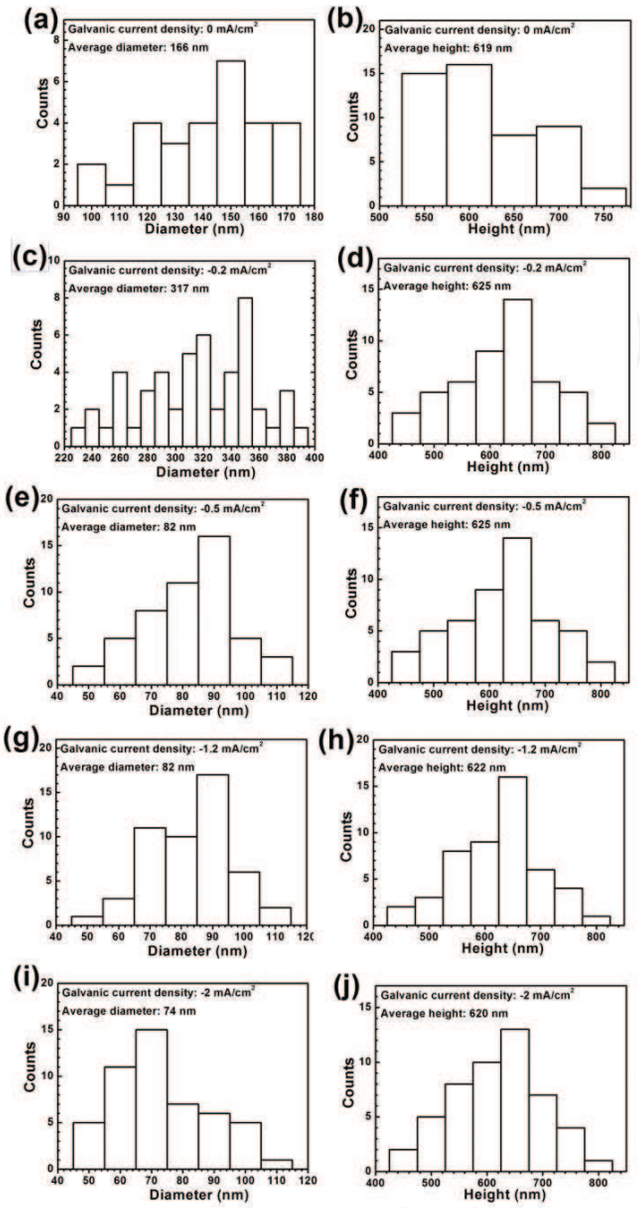

Figure 7. The diameter and height dispersion of the ZnO nanorods prepared by using two-stage electrodeposition method with the galvanic current density of 0 mA/cm^2 (a), (b); −0.2 mA/cm^2 (c), (d); −0.5 mA/cm^2 (e), (f); −1.2 mA/cm^2 (g), (h) and −2 mA/cm^2 (i), (j).

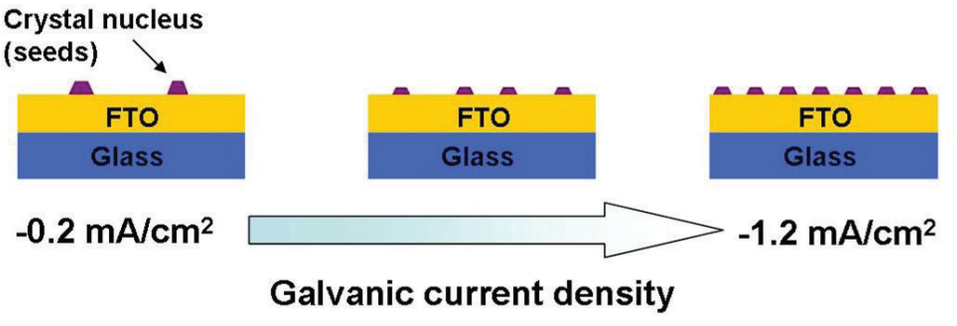

Figure 8. The sketch of the ZnO nanorods' nucleation mechanism under different galvanic current densities.

current density, the density of the nucleation sites was boosted from 1.5×10^9 to 2.4×10^9 1/cm^2. These nucleation sites assisted the following growth of ZnO nanorods with a higher density.

An increase in the galvanic current density, on the other hand, induced a significant decrease of the ZnO nanorods' average diameter. The average diameter of ZnO nanorods was reduced from 317 to 74 nm as the galvanic current density was increased from −0.2 to −2 mA/cm^2. The size of ZnO nanorods' diameter depended on the nucleation sites at the initial stage. Since the yields of OH^- ions is higher than Zn^{2+} ions in the initial process under a higher galvanic current density, the fact that the rate of OH^- generation is larger than the diffusion rate of Zn^{2+} ions to the cathode suppresses the lateral growth of the nucleation sites. As a consequence, the size of the nanorods' diameter was decreased by using a higher galvanic current density. The galvanic current did not lead to a significant variation of the ZnO nanorods' average length and the ZnO nanorods keep a virtually constant average length around 620 nm.

Galvanic current density (mA/cm^2)	Time (s)	Density (10^9/cm^2)
−0.2	40	–
−0.5	40	1.5
−1.2	40	2.7
−2	40	2.4

Table 6. Growth parameters and density of the samples prepared under a galvanostatic mode.

4. Conclusion

Thin-film photovoltaic device technology relies on light management to enhance light absorption in thin absorber layers. The use of the ZnO nanorods in the thin-film solar cells is an effective way to decrease the reflection. The variation of the geometrical parameters of the ZnO nanorods, such as the diameter, the height and the density can lead to an optimum, which results in the maximal absorption in the absorber. An approach of a rigorous modeling is presented to simulate and optimize the light absorption in the Cu(In,Ga)Se_2 absorbers with ZnO nanorods.

ZnO nanorod arrays were fabricated by using an electrochemical deposition method. A two-stage electrodeposition method for adjusting the ZnO nanorods' density on bare SnO_2:F substrates has been described and analyzed. The ZnO nanorods' density arrays were adjusted from 4.2×10^8 to 1.3×10^9 1/cm^2 by increasing the galvanic current density from −0.2 to −2 mA/cm^2. An increase in the galvanic current density induced a significant decrease of the ZnO nanorods' average diameter.

In this chapter, the modeling results show that the use of the ZnO nanorod arrays lead to an increase of the absorption in the absorber layer. After that, the growth of the ZnO nanorod arrays is tailored towards the optimized shape and geometry of the nanorod arrays. The opening questions and further research suggestions are outlined as follows.

The nanorods in the simulation are vertically aligned on the substrate. However, the real ZnO nanorods grown on FTO substrates are randomly oriented. It is suggested to run simulation on a tilted nanorod, which reflects the average orientation situation of the nanorod arrays. It is suggested to develop more effective ways to tailor the morphology and geometry of the ZnO nanorod arrays. Besides the use of the nanorods in the traditional thin-film solar cells, there are other possible methods for improving the light management in the thin-film solar cells. For example, some metal nanoparticles such as silver and gold nanodots can be incorporated into the solar cells. Due to the surface plasmonic effects of the nanoparticles, light will be efficiently coupled into the solar cells. In addition, a nanostructured antireflective coating layer can be coated on the surface of the cover glass in the thin-film solar modules. The antireflective coating layer will decrease the reflection between the glass and the air resulting in the boost of the light harvesting in the internal solar cells. The modern technology of the light management of the thin-film solar cells is now developing rapidly and the combination of the nanostructures and thin films will show the power.

Acknowledgements

This work was supported by the National Natural Science Foundation of China under Grant No. 61404007 and the Beijing Talents Fund (2015000021223ZK38).

Author details

Yang Tang

Address all correspondence to: tangy118@hotmail.com

National Institute of Clean-and-Low-Carbon Energy, Future Science & Technology City, Beijing, People's Republic of China

References

[1] ZSW, Press release, June 15, 2016.

[2] First Solar, Press release, February 23, 2016.

[3] C. W. Bunn, Proc. Phys. Soc. London 47, 835, 1935.

[4] R. B. Heller, J. McGannon, and A. H. Weber, J. Appl. Phys. 21, 1283, 1950.

[5] T. J. Gray, J. Am. Ceram. Soc. 37, 534, 1954.

[6] G. P. Mohatny and L. V. Azaroff, J. Chem. Phys. 35, 1268, 1961.

[7] R. R. Reeber, J. Appl. Phys. 41, 5063, 1970.

[8] Ü. Özgür, Y. I. Alivov, C. Liu, et al., J. Appl. Phys. 98, 041301, 2005.

[9] M. Law, L. E. Greene, J. C. Johnson, et al., Nat. Mater. 4, 455–459, 2005.

[10] X. W. Sun, J. Chen, J. L. Song, D. W. Zhao, W. Q. Deng, and W. Lei, Opt. Expr. 18(2), 1296–1301, 2010.

[11] D. C. Olson, S. E. Shaheen, R. T. Collins, et al., J Phys. Chem. C. 111, 16670–16678, 2007.

[12] M. Izaki and T. Omi, Appl. Phys. Lett. 68, 2439–2440, 1996.

[13] M. Izaki and T. Omi, J. Electrochem. Soc. 143, L53–L55, 1996.

[14] C. J. Lan, H. Y. Cheng, R. J. Chung, J. H. Li, K. F. Kao, and T. S. Chin, J. Electrochem. Soc. 154, D117–D121, 2007.

[15] J. Yang, Y. Qiu and S. Yang, Cryst. Growth Des. 7, 2562–2567, 2007.

[16] J. Chen, L. Ae, Ch. Aichele, and M. Ch. Lux-Steiner, Appl. Phys. Lett. 92, 161906, 2008.

[17] L. Vayssieres, K. Keis and S. E. Lindquist, J. Phys. Chem. B, 105, 3350, 2001.

[18] L. Schmidt-Mende and J. L. MacManus-Driscoll, Mater. Today, 10, 40, 2007.

[19] M. N. R. Ashfold, R. P. Doherty, N. G. Ndifor-Angwafor, D. J. Riley, Y. Sun, Thin Solid Films, 515, 8679, 2007.

[20] K. Govender, D. S. Boyle, P. B. Kenway, and P. O'Brien, J. Mater. Chem. 14, 2575, 2004.

[21] L. E. Greene, M. Law, and J. Goldberger, Angew. Chem. Int. Ed. 42, 3031–3034, 2003.

[22] Y. Tak and K. Yong, J. Phys. Chem. B, 109, 19263–19269, 2005.

[23] C-C Lin, H-P Chen, H-C Liao, et al. Appl. Phys. Lett. 86, 183103, 2005.

[24] V. S. Bagotsky, Fundamentals of Electrochemistry, John Wiley & Sons, Inc., New Jersey, 2006, Second edition, p. 22.

[25] S. B. Sadale, P. S. Patil, Solid State Ionics. 167, 273–283, 2004.

[26] A. I. Inamdar, Y. S. Kim, J. S. Sohn, H. Im, H. Kim, D.-Y. Kim, R. S. Kalubarme, C. J. Park, J. Korea Phys. Soc. 59, 145–149, 2011.

[27] A. I. Inamdar, S. H. Mujawar, S. B. Sadale, A. C. Sonavane, M. B. Shelar, P. S. Shinde and P. S. Patil, Sol. Energy Matar. Solar Cells. 91, 864, 2007.

[28] Y. Lin, J. Yang, X. Zhou, Appl. Surf. Sci. 258, 1491–1494, 2011.

[29] L. Vayssieres, K. Keis, S.-E. Lindquist, A. Hagfeldt, J. Phys. Chem. B, 105, 3350–3352, 2001.

IntechOpen